

BIELEFELD UNIVERSITY

MASTERS THESIS

Simulating sedation-induced unconsciousness in a Neural-Mass-Model

Author:
Felix FRIESE

Supervisor:
Dr. Malte SCHILLING

Examiner:
Prof Dr. Helge RITTER

*A thesis submitted in fulfillment of the requirements
for the degree of Master of Science*

in the

Neuroinformatics Group
Faculty of Technology

June 17, 2022

BIELEFELD UNIVERSITY

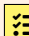
*Abstract*Faculty of Technology
Neuroinformatics Group

Master of Science

Simulating sedation-induced unconsciousness in a Neural-Mass-Model

by Felix FRIESE

Patients with severe Traumatic Brain Injuries (TBI) often remain in a state of unresponsive wakefulness. Brain-Computer-Interface (BCI)-based systems promise to improve the state assessment and to open a communication channel for patients to express their intent while in conscious states. Developing such a BCI-System (e.g. with EEG), including the necessary algorithms to assess a patients current wakefulness or consciousness state from EEG data is a challenging task. Development, testing and evaluation of these algorithms requires labeled data (ground truth), which is almost impossible to obtain given the patients' lack of communication capabilities. Therefore, it would be desirable to generate a synthetic signal, which should ideally resemble real EEG data in all relevant features. We previously developed a simple ICA-based model, which generates a multichannel EEG from base-signals with configurable spectral features. While this proved useful for testing numerous components of our signal-analysis framework, it lacks biological plausibility and explanatory power to model the changes in the signal's properties given an altered state of consciousness. In this thesis, we propose an approach towards overcoming these issues while sticking with the original goal of generating realistic, practically useful surrogate data. A biologically motivated Neural Mass Model (NMM) on cortical-column level is implemented, which is able to approximate the effects of sedation-induced unconsciousness on the generated signal. The model is then shown to be able to reproduce the characteristic effects that sedation has on the EEG-Signals of real subjects. This is a first step to a model of consciousness-altering processes in the brain, which could ultimately be extended to realistically simulate other processes like sleep and trauma-induced DoC, facilitating better detection algorithms and furthering the goal to develop working BCI-Systems in the given context.

 Todo

This is old! Re-write the abstract to match the new hypothesis! (very last thing to do)

Contents

Abstract	iii
1 Introduction	1
1.1 Motivation	1
2 Technical Concepts	3
2.1 General Anaesthesia	3
2.1.1 Basics	3
2.1.2 Units for propofol concentration	3
2.1.3 Realistic propofol concentrations during general anaesthesia (GA)	3
2.1.4 Effects of propofol on the IPSP	3
2.1.5 Hysteresis of propofol	4
2.2 EEG	6
2.2.1 Measurement	6
2.2.2 Advantages/Disadvantages	6
2.2.3 States of Consciousness in the EEG Signal	6
2.2.4 Biphasic Effect	6
2.2.5 Simulation	6
2.2.5.1 Motivation	6
2.2.5.2 Approaches	6
2.2.5.3 Model Choice	6
2.3 Neural Mass Models	7
2.3.1 The Jansen-Rit Model	7
2.3.1.1 Potential-To-Rate Block	8
2.3.1.2 PSP-Blocks	9
2.3.1.3 Full Linear System	12
2.3.1.4 Connectivity Constants	12
2.3.1.5 Model Input	13
2.3.1.6 Model Output	13
2.3.2 The David and Friston Model	15
2.3.2.1 Introducing sub-populations	15
3 Methodology	19
3.1 PyRates Framework	19
3.1.1 Implementation of the Jansen-Rit Model	19
3.1.2 Implementation of Subpopulations	20
3.2 Simulating the effects of propofol	21
3.3 Implementing decay-time modulation	21

4	Results	23
4.1	Simulating over the parameter space	23
4.1.1	Basic JR Model	24
5	Discussion	25
5.1	Outlook	25
	Bibliography	27

List of Abbreviations

BCI	B rain C omputer I nterface
DoC	D isorder(s) o f C onsciousness
EEG	E lectroencephalography
fMRI	f unctional M agnetic R esonance I maging
GA	G eneral A naesthesia
GABA	G amma- A minobutyric A cid
ICA	I ndependent C omponent A nalysis
[E/I]IN	[E xcitatory/ I nhibitory] I nter n euron
[L/R]OC	[L oss/ R ecovery] O f C onsciousness
NMM	N eural M ass M odel
PC	P yramidal C ell
[E/I]PSP	[E xcitatory/ I nhibitory] P ost- S ynaptic- P otential
TBI	T raumatic B rain I njury

Chapter 1

Introduction

1.1 Motivation

The highly complex processes of changing states of consciousness in the human brain are still barely understood. States of consciousness have historically been defined based on behavioral observations such as responsiveness to stimuli. As no other indications, save simple physiological measurements such as pulse and respiration rate, were available, the concept of awareness was tightly linked to observable behavior. While the great majority of medical applications to determine levels of consciousness, even in practical clinical contexts [42], are still covered by these observations, there are cases in which the link between consciousness and displayed behavior falls apart; striking examples are some disorders of consciousness (DOC) as well as the total locked-in syndrome [6], where patients are unable to display any visible behavior, while maintaining some or even full awareness. Although cases like these are rare, they highlight that consciousness needs to be studied at its source – on the level of brain-activity – to fully understand the mechanisms that lead to its different states. Brain-activity can be measured directly or indirectly. Direct measurement with electrodes in the brain, while more accurate, poses the obvious problem of its invasive nature and faces the challenge of realistically

☰ Todo rephrase

only allowing very localized measurements [citation needed]. Various neuroimaging techniques, which indirectly measure brain-activity, have been used to study levels of awareness since their emergence. Already in the 1880's, Angelo Mosso measured scalp-pulse variations in subjects with skull-injuries during challenging tasks, and concluded an increased blood-flow to the brain [1]. Improved techniques like the fMRI and the EEG allow for non-invasive observation of brain-activity and have been used extensively to study the dynamics of the brain during sleep and loss and return of consciousness [citation needed]. Some phenomena, like predictable changes in signal-frequencies and some critical brain regions involved in consciousness-modulation have been identified and are well documented [citation needed]. Techniques to measure levels of consciousness via neuroimaging have been proposed [9], [25] and used in practise [43]. However, exact mechanisms behind state-changes are still object of fundamental research.

Controlled state-changes, like inducing loss-of-consciousness with anaesthetic drugs, are exceptionally well-suited for studying the underlying mechanisms of consciousness, as they allow for repeatable conditions. Furthermore, the neuro-chemical mechanisms of the drugs provide a good starting-point for modeling these processes. The sedative propofol is the most commonly used drug to induce controlled loss of consciousness

during general anaesthesia. Propofol's neuro-chemical mode of action and its specific effects on synaptic receptors are well understood, which lays a solid foundation to study the brain-dynamics associated with loss of consciousness.

A promising approach to further our insights step by step, is to simulate controlled state-changes (such as anaesthesia) in computer-models to develop an understanding of the dynamics of brain-activity and its effects on consciousness. Computer-models of the brain (or parts of it) exist on different levels [41], including simulations of individual neurons and population-based approaches. Neural-Mass-Models (NMMs), members of the latter, model synaptic connections between populations of different types of neurons and have proven to replicate multiple abstract phenomena of brain-dynamics[28], [31] within a small cortical column. The simplifications they provide allow efficient real-time simulation of signals, while preserving many important characteristics of EEG or MEG signals.

☰ Todo improve explanation of NMMs

By combining the well-known properties of propofol with an NMM, we can hope to gain insights into the mechanisms that govern changes of brain-dynamics in the presence of consciousness-altering drugs. While the abstract nature of NMMs, along with its limitations must always be considered [40], the results of simulated experiments can provide valuable research indications.

One of the most commonly used models in the area of neural population models is the Jansen-Rit [10] (JR) NMM, which is based on efforts by Wilson & Cowan [2], Lopes da Silva et al. [3], [4] and Zetterberg et al. [5]. It is one of the most simple and basic population models, while retaining 'a considerable degree of biological realism' and 'producing a surprisingly rich repertoire of dynamic behaviors' [31]. Many efforts in the field are based on the JR NMM, e.g. [13], [16], [21], [23], [29], [36] and others.

Neural-Mass models have been widely used to simulate the properties of different states of consciousness. Cona et al. [29] adapted the JR NMM to simulate effects of different stages of sleep. Their model accounts for thalamo-cortical modulation of cortico-cortical connectivity as an important mechanism to influence these transitions. Bensaid et al.'s COALIA Framework [36], makes use of a similar structure, while using over 60 interconnected NMM-modules and applying a transformation onto scalp electrodes using a realistic head-model with tissue conductivities.

As we are looking to simulate propofol-induced unconsciousness, similar approaches bear special consideration: To simulate phenomena specific to general anaesthesia, Steyn-Ross et al. [18], [24] developed a model based on Liley et al.'s continuum model [12].

☰ Todo short explanation of continuous cortical field theories CFT, the difference to 'normal' NMMs

This work aims to use a non-CFT approach based on the JR model and evaluate if it is able to reproduce the behavior observed in Steyn-Ross et al.'s CFT model [24]. While the basic JR model is able to produce rich patterns of dynamic behavior [23], large regions of its parameter-space generate sinusoidal signals with a single pronounced frequency, which might limit its ability to reproduce the expected phenomena (as noted by [34]). Therefore, the subpopulation-extension proposed by David & Friston [16] is also employed to produce a more realistic baseline frequency spectrum.

Chapter 2

Technical Concepts

2.1 General Anaesthesia

2.1.1 Basics

General Anaesthesia is usually employed in surgical contexts to keep patients from experiencing the pain of the operation. Sedative drugs are carefully administered to the patient by trained practitioners to induce loss of consciousness, without causing permanent damage to the brain or other parts of the body

2.1.2 Units for propofol concentration

Some papers [19] cite propofol concentrations in $\frac{\mu\text{g}}{\text{mL}}$, while others [17], [20] use μM (micromolar = $\frac{\mu\text{mol}}{\text{L}}$). To get comparable numbers, we first need to establish the following relation for Propofol (molar mass: 178.27 g):

$$1 \frac{\mu\text{g Propofol}}{\text{mL}} = \frac{1 \frac{\mu\text{g}}{\text{mL}}}{178.27 \frac{\text{g}}{\text{mol}}} = 5.609 \mu\text{M}$$

In this work, we will settle on μM and only mention values in $\frac{\mu\text{g}}{\text{mL}}$ where they are taken from a source, but then provide the converted value as well.

2.1.3 Realistic propofol concentrations during general anaesthesia (GA)

During GA, effect-site concentrations (c_e , concentration near the synaptic receptors) of propofol may easily range up to $5 \frac{\mu\text{g}}{\text{mL}}$ ($\approx 28 \mu\text{M}$). Loss of Consciousness (LOC) occurs on average at $c_e \sim 2.0 \frac{\mu\text{g}}{\text{mL}}$ ($\approx 11.2 \mu\text{M}$), while the Recovery of Consciousness (ROC) averages at $c_e \sim 1.8 \frac{\mu\text{g}}{\text{mL}}$ ($\approx 10.1 \mu\text{M}$). Both values may vary substantially for individual subjects. LOC has a strong tendency to occur at higher concentrations than ROC [19], [38]. Throughout GA, effect-site concentration is commonly derived from measured blood-plasma concentration (c_p) using more or less complex Pharmacokinetic (PK)-Models (e.g. [30], [32]), as direct measurement is impractical for obvious reasons. Since our model will work with c_e directly, we will disregard this for now - however, it should be kept in mind.

2.1.4 Effects of propofol on the IPSP

Research on the effect of propofol on the IPSC (Inhibitory Post-Synaptic Current) and EPSC has shown that propofol strongly affects the IPSP decay time [17], [20]. The EPSP and the amplitude of the IPSP are unaffected by propofol. Effect-site

concentrations at clinically relevant levels increase the IPSP decay time significantly (e.g. around 10 μM the decay time roughly doubles) [17].

Using the data-points from [17] and assuming a very rough manual logarithmic fit (see Fig. 2.1), the function

$$\mathcal{D}(c_e) = 0.65 * \ln((c_e/2) + 1) + 1$$

will be used to calculate the decay-time factor λ from a given effect-site concentration in μM .

As there unfortunately were only a few data-points (and none above 10 μM , leaving a large part of the relevant parameter space empty), a computational model-fit might have over-valued those points. A visually fitted logarithmic function (assuming eventual effect saturation) seemed like a sensible choice for this use-case. However, since inter-subject variations are substantial in any case, the exact values do not matter as much as the order of magnitude.

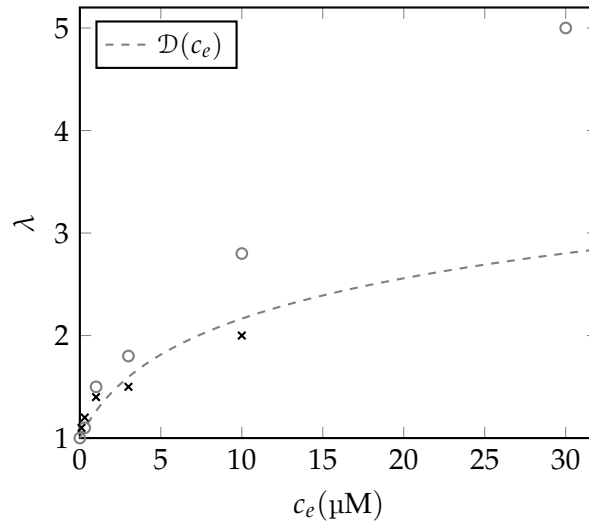


Figure 2.1: very rough manual logarithmic fit of decay-time factor to measured values from [17].

2.1.5 Hysteresis of propofol

If the state of a system depends not only on its parameters, but also the systems history, this dependency is called hysteresis. The human body often reacts differently to the same concentration of a drug, depending on whether the concentration is rising or decaying. Hysteresis is well documented during propofol-induced GA [11], [19], [35], [38], [39]. The most prominent effect being a counter-clockwise hysteresis for LOC and ROC (as mentioned in 2.1.3). The effects on responsiveness of subjects usually start at higher concentrations than they end. While some of that effect might be caused by inaccurate PK-Models, misgauging the actual effect-site concentration, there is a growing body of research that supports the notion that the observed effect is independent of pharmacokinetic interference [24], [39].

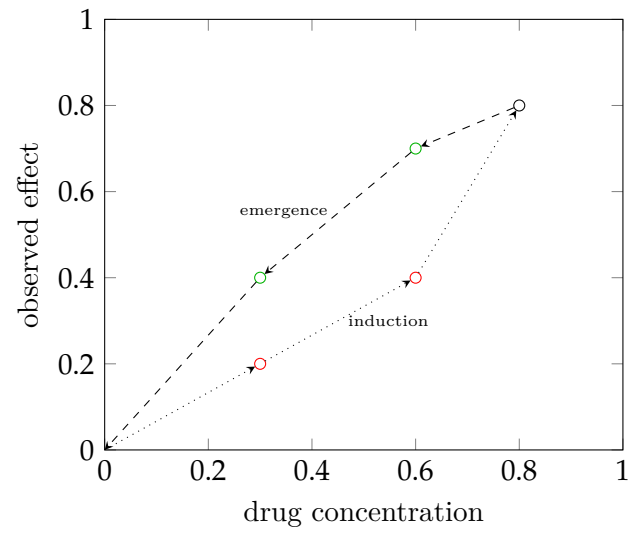
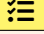



Figure 2.2: Example of counter-clockwise drug hysteresis

2.2 EEG


2.2.1 Measurement

 **Todo** how the EEG is measured technically and which neuronal processes it actually observes (signal amplification, pyramidal cells, ...)

2.2.2 Advantages/Disadvantages

 **Todo** spatial/temporal resolution, invasiveness, ...

2.2.3 States of Consciousness in the EEG Signal


 **Todo** how do the states differ in the signal

2.2.4 Biphasic Effect


A biphasic effect (an initial increase of an effect, that decreases with higher concentrations) in the EEG can be observed for many sedatives [11], [14]. For propofol, a temporary steep increase in EEG amplitude in the 2–20 Hz ranges, loosely correlated with the onset of LOC, as well as ROC can be observed.

2.2.5 Simulation


2.2.5.1 Motivation

 **Todo** what can we hope to achieve by simulating an EEG signal

2.2.5.2 Approaches

 **Todo** which tools are at our disposal (naive frequency mixing, population models, simulating individual neurons, ...)

2.2.5.3 Model Choice

 **Todo** argue about models \Rightarrow why did we land on NMMs/population models?

2.3 Neural Mass Models

Todo

slightly deeper introduction (we already have this in the EEG section) to NMMs in general

2.3.1 The Jansen-Rit Model

The widely used Jansen-Rit Model [8], [10], is based on earlier models by Wilson & Cowan [2], Lopes da Silva et al. [3], [4] and Zetterberg et al. [5]. It represents a cortical column in the brain, which is made up of three main components, each modeling a population of neurons with distinct characteristics.

The basic schema of the model is visualized in Fig. 2.3, showing the connections between the main components. There is a population of Pyramidal Cells which receives input from two populations of inter-neurons, one of which is excitatory while the other is inhibitory. Each of the inter-neuron-populations receives the output of the PC population. Additionally, there is external excitatory input to the PC population from other regions of the brain.

The Block Diagram (Fig. 2.4) shows the individual modules of the model. A population consists of two types of blocks: The *PSP-Block* models the behavior of the synapses and neuronal somata. It can be either excitatory or inhibitory and converts the incoming average pre-synaptic pulse density to an average post-synaptic membrane potential by convolving it with an impulse response function ($h_e(t)$ and $h_i(t)$, for excitation and inhibition respectively). The second block (sometimes called *Potential-To-Rate-Block* after it's functionality) calculates the populations response to this stimulation, transforming the incoming average membrane potential back into an average pulse density of action potentials. It may be roughly viewed as a functional counterpart to the axon hillock by establishing a firing threshold and is usually implemented by a Sigmoid Function (*Sigm*). External input from other regions of the brain is represented by $p(t)$. The Connectivity Constants C_1 , C_2 , C_3 and C_4 are a proportional representation of the average number of synapses between the populations. The signal most closely related to the EEG and therefore the variable of interest, is the summed average membrane potential of the PC population ($y_1(t) - y_2(t)$ in Fig. 2.4).

Todo

explain neurophysiology why $EEG \approx y_1 - y_2$, or reference back to explanation in EEG section

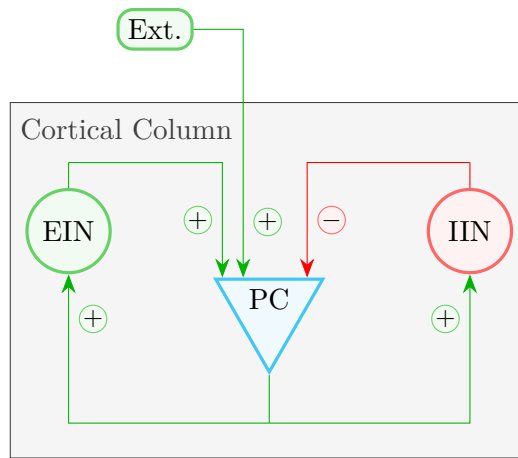


Figure 2.3: Basic Schema of the Jansen-Rit Model: Three populations of neurons

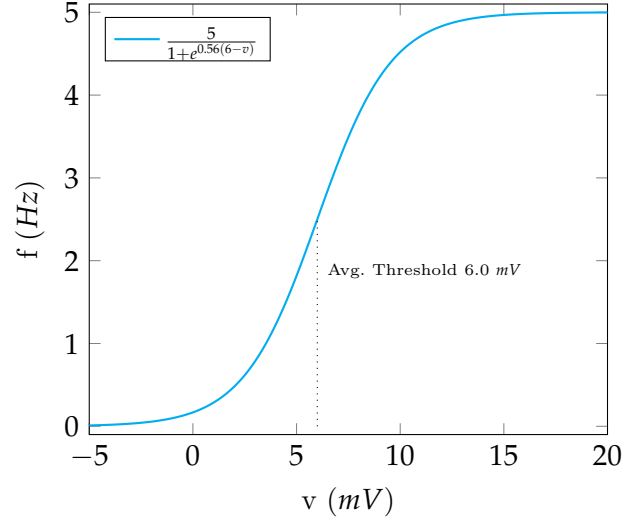


Figure 2.5: Sigmoid (Eq. 2.1) [8]

2.3.1.2 PSP-Blocks

In Physics, Linear Time-Invariant Systems (LTI systems) are oftentimes used to describe the response of electrical circuits to arbitrary input signals. They consist of a kernel function (or impulse-response function), that models the system's response to a single unit-impulse. The PSP-Blocks are an LTI system, fully represented by an impulse response function. It describes a PSP relative to the onset of a pulse. Since the PSP differs depending on the type of cell (excitatory or inhibitory), there are two different impulse-response functions. The parameters for the EPSP (Eq. 2.2) and IPSP (Eq. 2.3) are given in Table 2.2. The respective plots are visualized in Fig. 2.6.

Parameter		Default Value	Unit
Exc. max. amplitude / e	A	3.25	mV
Lumped repr. of sum of exc. delays	a	100	Hz
Inh. max. amplitude / e	B	22	mV
Lumped repr. of sum of inh. delays	b	50	Hz

Table 2.2: Parameters of the PSP Blocks

Excitatory impulse response:

$$h_e(t) = \begin{cases} Aate^{-at} & t \geq 0 \\ 0 & t < 0 \end{cases} \quad (2.2)$$

Inhibitory impulse response:

$$h_i(t) = \begin{cases} Bbte^{-bt} & t \geq 0 \\ 0 & t < 0 \end{cases} \quad (2.3)$$

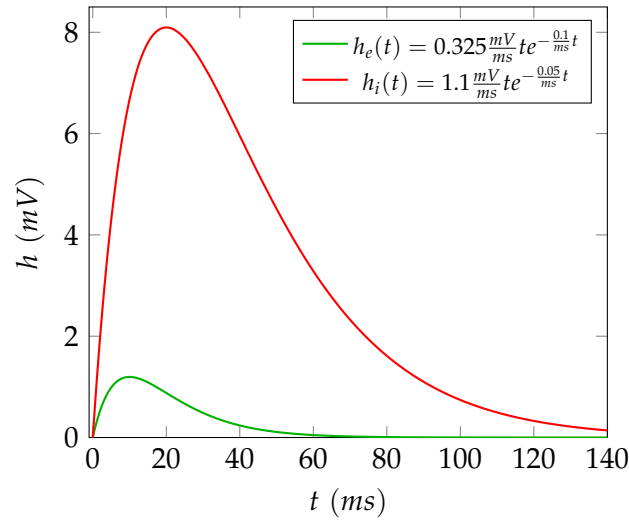


Figure 2.6: Impulse Response Functions: Note the small EPSP (Eq. 2.2) and the large IPSP (Eq. 2.3) [8]

Jansen and Rit [8] justify the difference in amplitude by referencing Lopes da Silva et al. [4] and stating that inhibitory neurons synapse closer to the somata of pyramidal cells (often on the cell body) than excitatory cells, increasing the effect of an inhibitory neuron about 10-fold.

☰ Todo maybe go more into detail about the reasons for stronger inhibition

The output of the Linear System defined by the PSP-Blocks is calculated by a convolution (denoted by $*$) of the incoming impulse density $x(t)$ with the impulse response function $h(t)$ (Eq. 2.4).

Remark (Convolution). The convolution of two functions $f(t)$ and $g(t)$ is defined as the integral of their product after one function has been reversed and shifted ¹:

$$f(t) * g(t) = \int_{-\infty}^{+\infty} f(\tau)g(t - \tau)d\tau$$

If $f(t)$ is a unit-impulse $\delta(t)$ (in our case that would mean each cell of the previous population firing a single action potential at the same time) the result is just $g(t)$ (in our case representing a single full-amplitude impulse response as the mean membrane potential):

$$\delta(t) * g(t) = \int_{-\infty}^{+\infty} \delta(\tau)g(t - \tau)d\tau = g(t)$$

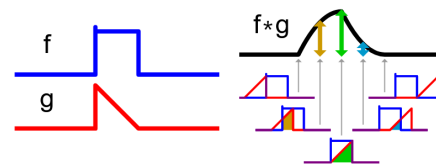


Figure 2.7: Convolution: The area enclosed by $f(\tau)$ and $g(t - \tau)$ is the value of $(f * g)(t)$.

By Cmglee - Own work, CC BY-SA 3.0
<https://commons.wikimedia.org/w/index.php?curid=20206883>

¹There is a very intuitive explanation of convolutions by Kalid Azad on his website <https://betterexplained.com/articles/intuitive-convolution/>

In the general case, this process can be used to mathematically model the integration of incoming action potential densities in the soma.

Importantly, the Convolution Theorem states that the convolution of $f(t)$ and $g(t)$ becomes a simple multiplication when applying the Laplace Transform:

$$\mathcal{L}\{f(t) * g(t)\} = \mathcal{L}\{f(t)\}\mathcal{L}\{g(t)\} = F(s)G(s)$$

That means you can calculate a convolution with the inverse Laplace-Transform of the multiplication of the functions' individual Laplace-Transforms:

$$f(t) * g(t) = \mathcal{L}^{-1}\{F(s)G(s)\}$$

Since the convolution in the time-domain is a computationally heavy operation, it is oftentimes faster to transform the equation into the Laplace-Domain (see Eq. 2.5), apply the Convolution Theorem and perform the multiplication there, and transform the results back to the time-domain. This results in a second order differential equation (Eq. 2.6) that can be efficiently solved by numerical integration. To obtain this form, we need the Laplace transform $H_e(s)$ (in this context also called *Transfer Function*) of our response function $h_e(t)$:

$$H_e(s) = \mathcal{L}\{h_e(t)\} = \mathcal{L}\{Aate^{-at}\} = \frac{Aa}{(s+a)^2} = \frac{Aa}{s^2 + 2as + a^2}$$

With that, we can start to transform our initial equation into the desired Second Order System:

$$\underbrace{y(t)}_{\text{PSP}} = \underbrace{h_e(t)}_{\text{impulse response}} * \underbrace{x(t)}_{\text{impulse density}} \quad (2.4)$$

applying the Laplace-Transform eliminates the convolution:

$$\begin{aligned} \xleftrightarrow{\mathcal{L}} \quad Y(s) &= \underbrace{H_e(s)}_{\text{transfer function}} \cdot X(s) & (2.5) \\ \iff Y(s) &= \frac{AaX(s)}{s^2 + 2as + a^2} \\ \iff (s^2 + 2as + a^2)Y(s) &= AaX(s) \\ \iff s^2Y(s) + 2asY(s) + a^2Y(s) &= AaX(s) \end{aligned}$$

reversing the Laplace-Transform yields a differential equation in the time domain:

$$\begin{aligned} \xleftrightarrow{\mathcal{L}^{-1}} \quad \ddot{y}(t) + 2a\dot{y}(t) + a^2y(t) &= Aax(t) \\ \iff \ddot{y}(t) &= Aax(t) - 2a\dot{y}(t) - a^2y(t) & (2.6) \end{aligned}$$

which can be expressed as a system of two coupled first order equations:

$$\dot{y}(t) = z(t) \quad (2.7)$$

$$\dot{z}(t) = Aax(t) - 2az(t) - a^2y(t) \quad (2.8)$$

where $y(t)$ is the resulting PSP and $x(t)$ the incoming pulse density. This works analogously for the inhibitory case with $h_i(t)$.

2.3.1.3 Full Linear System

Taking the two first order equations for $\dot{y}(t)$ (Eq. 2.7) and $\dot{z}(t)$ (Eq. 2.8), and the Block diagram (Fig. 2.8) as a base, we can now state the equations for the full Jansen-Rit Model with it's three populations. Each PSP-Block $h(t)$ needs it's own system of coupled differential equations. The value of $x(t)$ can be easily taken from the Block Diagram. $y_0(t)$ is the EPSP received by both the EIN and IIN population, while $y_1(t)$ is the EPSP and $y_2(t)$ the IPSP received by the PC population:

$$\begin{aligned}
 \dot{y}_0(t) &= z_0(t) \\
 \dot{z}_0(t) &= Aa\text{Sigm}[y_1(t) - y_2(t)] - 2az_0(t) - a^2y_0(t) \\
 \dot{y}_1(t) &= z_1(t) \\
 \dot{z}_1(t) &= Aa(p(t) + C_2\text{Sigm}[C_1y_0(t)]) - 2az_1(t) - a^2y_1(t) \\
 \dot{y}_2(t) &= z_2(t) \\
 \dot{z}_2(t) &= Bb(C_4\text{Sigm}[C_3y_0(t)]) - 2bz_2(t) - b^2y_2(t)
 \end{aligned} \tag{2.9}$$

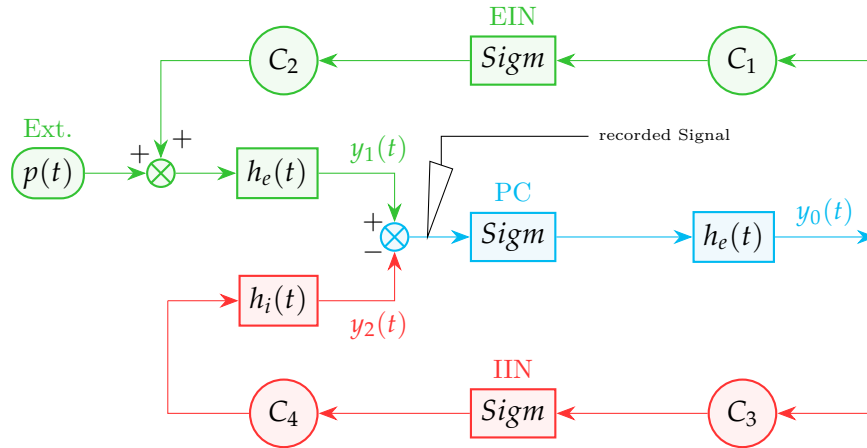


Figure 2.8: Colored Block diagram, visualizing the components of (Eq. 2.9)

2.3.1.4 Connectivity Constants

A sensible choice for the Connectivity Constants C_1 to C_4 was determined by Jansen and Rit empirically by defining a histologically motivated relationship between them ($C = C_1 = \frac{C_2}{0.8} = \frac{C_3}{0.25} = \frac{C_4}{0.25}$) and varying C until the system produced the desired natural alpha-like activity at $C = C_1 = 135 \Rightarrow C_2 = 108; C_3 = C_4 = 33.75$. Varying C can account for common synaptic phenomena like neurotransmitter depletion [10].

☰ **Todo** go more into detail about the biological motivation and the effects of these constants on the generated signal

2.3.1.5 Model Input

The model input $p(t)$ represents the average activity of populations outside the modeled column that synapse on the columns PC population. Since this activity's source is so diverse, it is modeled by white noise (120-320 Hz).

☰ Todo

go more into detail why the input is modeled like this

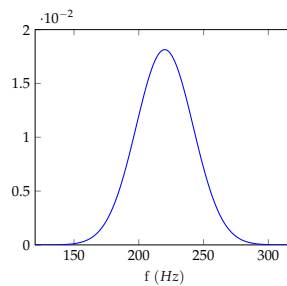


Figure 2.9: Input distribution. The input frequency representing $p(t)$ is sampled from a normal distribution with $\mu = 220$ and $\sigma = 22$

2.3.1.6 Model Output

The simulated data from $y_1 - y_2$ while varying C looks like this:

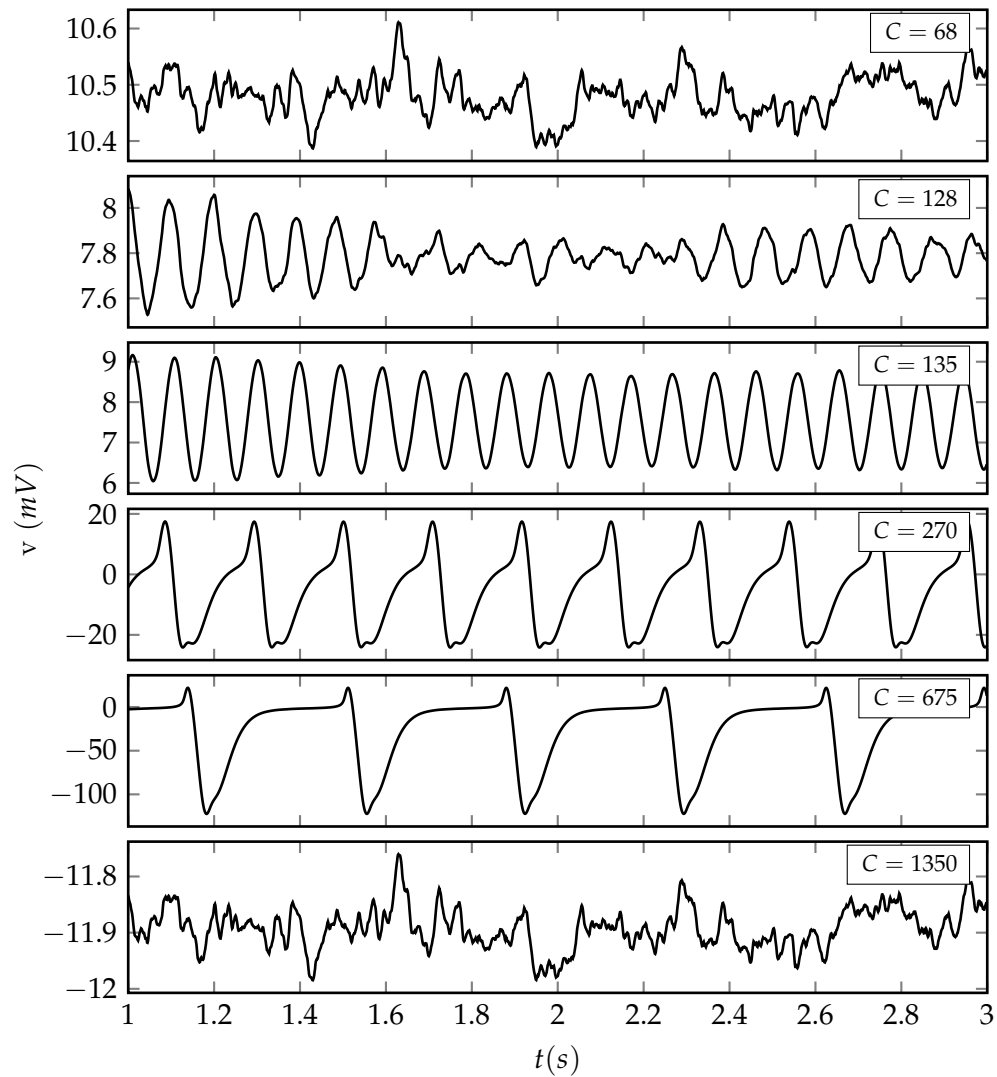


Figure 2.10: Model Output for varying C . Well defined alpha-activity is visible at $C = 135$.

Todo Explain Graph, generally provide more information to the systems output

2.3.2 The David and Friston Model

⚠ Section Incomplete

the whole David-Friston-Section is still very much preliminary

While the Jansen-Rit model succeeds in generating realistic alpha activity, real EEG Signals contain much richer spectra [15]. David and Friston [16] proposed a modification to the Jansen-Rit model, that could produce a more realistic frequency spectrum by introducing sub-populations to the model. They can be tuned individually to produce oscillations in different frequencies.

2.3.2.1 Introducing sub-populations

David and Friston slightly redefine $h(t)$ by introducing the parameters H and τ (see Table 2.3), which is just a minor alteration of A and a .

$$h(t) = Aate^{-at} \Rightarrow h(t) = \frac{H}{\tau}te^{-\frac{1}{\tau}t}$$

Furthermore, as they are tweaking these parameters to produce slower or faster sub-populations, they define the products $H_e\tau_e = 0.0325mVs$ and $H_i\tau_i = 0.44mVs$ as constants. This is done to preserve the oscillatory behavior of each population [16]. When varying τ , H is therefore adjusted accordingly ($H_e = \frac{0.0325mVs}{\tau_e}$, $H_i = \frac{0.44mVs}{\tau_i}$).

Parameter		Value	Unit	Relation to [10]
Excitatory delays	τ_e	0.01	s	$\tau_e = \frac{1}{a}$
Inhibitory delays	τ_i	0.02	s	$\tau_i = \frac{1}{b}$
Excitatory synaptic gain	H_e	3.25	mV	$H_e = A$
Inhibitory synaptic gain	H_i	22	mV	$H_i = B$

Table 2.3: Parameters of the PSP Blocks after [16]

Attention: From now on, the indices $[0, \dots, N]$ for y , h , τ and H refer only to the subpopulations within a single population. The indices used above in the formulation for the Simple Jansen-Rit Model (and the Block Diagram) should not be confused with these. However, e and i as indices still denote excitatory and inhibitory populations respectively.

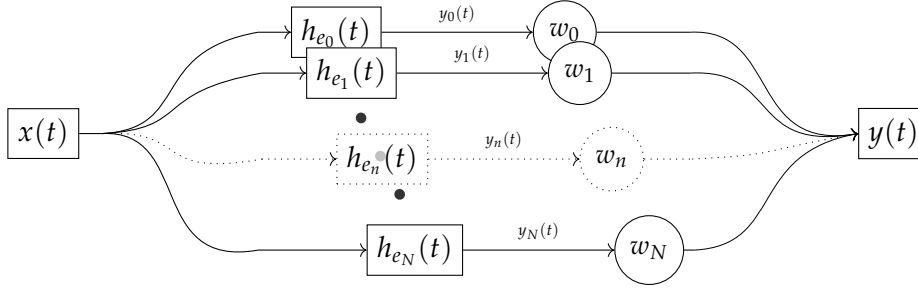


Figure 2.11: Example of subpopulations $(h_{e_0}(t), \dots, h_{e_N}(t))$ forming an excitatory population $h_e(t)$

By introducing subpopulations, we split up the general impulse response function $h(t)$ in N individual sub-functions:

$$h_n(t) = \frac{H_n}{\tau_n} t e^{-\frac{1}{\tau_n}}$$

The previously defined general PSP-Block Equation:

$$y(t) = h(t) * x(t)$$

then becomes:

$$y(t) = \sum_{n=0}^N (w_n \cdot h_n(t) * x(t)) \quad \text{with} \quad \sum_{n=0}^N w_n = 1 \quad \text{and} \quad 0 \leq w_n \leq 1$$

with N individually weighted (w_n) and parameterized ($h_n(t)$) subpopulations. We can then declare:

$$y_n(t) = h_n(t) * x(t) \quad \text{and} \quad y(t) = \sum_{n=0}^N (w_n y_n)$$

which produces the following differential equations for a single PSP Block:

$$\begin{aligned} \dot{y}_0(t) &= z_0(t) \\ \dot{z}_0(t) &= \frac{H_0}{\tau_0} x(t) - \frac{2}{\tau_0} z_0(t) - \left(\frac{1}{\tau_0}\right)^2 y_0(t) \\ &\dots \\ \dot{y}_N(t) &= z_N(t) \\ \dot{z}_N(t) &= \frac{H_N}{\tau_N} x(t) - \frac{2}{\tau_N} z_N(t) - \left(\frac{1}{\tau_N}\right)^2 y_N(t) \\ y(t) &= w_1 y_1 + \dots + w_N y_N \end{aligned} \tag{2.10}$$

David and Friston further propose an example with two subpopulations for each population with the following parameters: $\tau_{e_1} = 10.8ms$, $\tau_{i_1} = 22ms$, $\tau_{e_2} = 4.6ms$, $\tau_{i_2} = 2.9ms$. While the kinetics for the first subpopulation were still close to those of the original populations ($\tau_e = 10ms$, $\tau_i = 20ms$, which produce alpha activity), the second population's parameters were chosen to produce gamma activity.

☰

Todo

put the values in a table

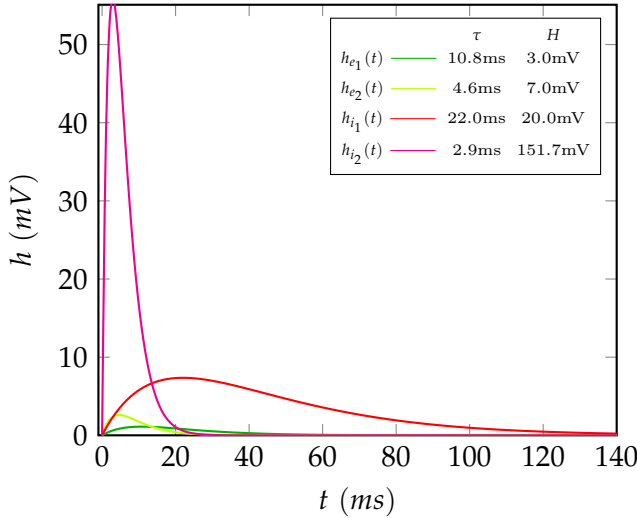


Figure 2.12: PSP functions for Subpopulations: — and — are faster subpopulations

Chapter 3

Methodology

3.1 PyRates Framework

⚠ Section Incomplete
preliminary

The whole PyRates section is still very much

The PyRates Framework is a Python software framework, written by Richard Gast and Daniel Rose at the Max-Planck-Institute in Leipzig. It can simulate a wide range of graph-representable neural models, while setting a focus on rate-based population models [37]. It wraps computational backends like Numpy and Tensorflow and offers predefined nodes and edges (components that model units like cells or cell populations and the connections between them with mathematical equations) to be used, replaced or extended with custom equations. Furthermore it provides two simple ways to define these components and the derived network configurations: either by YAML-File or within Python code. These configurations are then compiled into optimized executable code with respect to the chosen backend before being executed. It comes with pre-configured model-definitions for some of the most frequently used models, e.g. the basic Jansen-Rit Circuit [10] and the Montbrio-Model [33], as well as some variations thereof. It's ease of use, the fact that it could easily reproduce the characteristics of the basic Jansen-Rit model out of the box, and the open-source character made it a sensible choice for this thesis.

3.1.1 Implementation of the Jansen-Rit Model

PyRates works with population models by compositing multiple operators, like the PSP- (or Rate-To-Potential-) and Sigmoid- (or Potential-To-Rate) Block into nodes. These nodes represent populations that can then be connected via edges (synapses). For example one might combine two PSP-Blocks (for excitatory and inhibitory input respectively) with a Sigmoid Block to create a PC-Node. This node can then receive rate-input to each of it's PSP-Blocks and produces rate-output from it's Sigmoid-Block. The EIN- and IIN- nodes are functionally identical and just combine an excitatory PSP-Block with a Sigmoid Block. By connecting these Blocks (see Fig. 3.1) and adding random input to the excitatory PSP-Block of the PC-Node, the

simple Jansen-Rit Circuit is already complete.

$$\begin{aligned}
 \frac{d}{dt}PSP_{EIN} &= PSP_{t_{EIN}} \\
 \frac{d}{dt}PSP_{t_{EIN}} &= \boxed{\frac{H_e}{\tau_e} \cdot C_1 \text{Sigm}[PSP_{PC}] - \frac{2}{\tau_e} \cdot PSP_{t_{EIN}} - \left(\frac{1}{\tau_e}\right)^2 \cdot PSP_{EIN}} \\
 \frac{d}{dt}PSP_{IIN} &= PSP_{t_{IIN}} \\
 \frac{d}{dt}PSP_{t_{IIN}} &= \boxed{\frac{H_i}{\tau_e} \cdot C_3 \text{Sigm}[PSP_{PC}] - \frac{2}{\tau_e} \cdot PSP_{t_{IIN}} - \left(\frac{1}{\tau_e}\right)^2 \cdot PSP_{IIN}} \\
 \frac{d}{dt}PSP_{PC_E} &= PSP_{t_{PC_E}} \\
 \frac{d}{dt}PSP_{t_{PC_E}} &= \boxed{\frac{H_e}{\tau_e} \cdot (p(t) + C_2 \text{Sigm}[PSP_{EIN}]) - \frac{2}{\tau_e} \cdot PSP_{t_{PC_E}} - \left(\frac{1}{\tau_e}\right)^2 \cdot PSP_{PC_E}} \\
 \frac{d}{dt}PSP_{PC_I} &= PSP_{t_{PC_I}} \\
 \frac{d}{dt}PSP_{t_{PC_I}} &= \boxed{\frac{H_i}{\tau_i} \cdot C_4 \text{Sigm}[PSP_{IIN}] - \frac{2}{\tau_i} \cdot PSP_{t_{PC_I}} - \left(\frac{1}{\tau_i}\right)^2 \cdot PSP_{PC_I}} \\
 PSP_{PC} &= PSP_{PC_E} - PSP_{PC_I}
 \end{aligned} \tag{3.1}$$

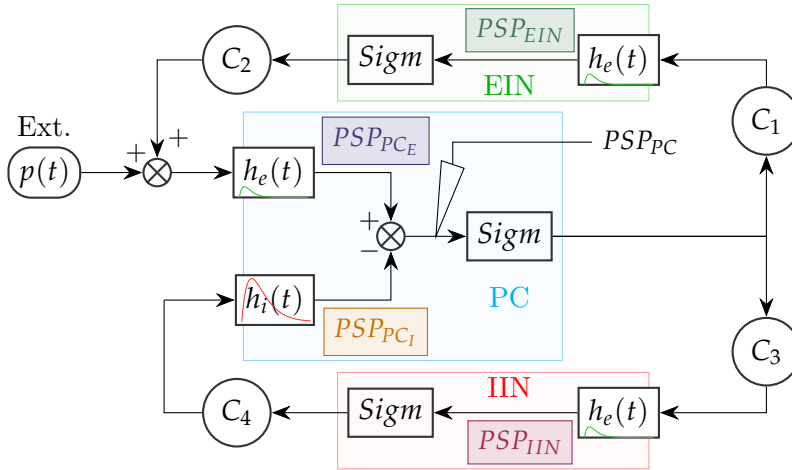


Figure 3.1: Jansen-Rit Block Diagram as implemented in PyRates: Each population can be clearly identified by one or more afferent PSP-Blocks and a single Sigmoid that calculates the populations output. This approach is more modular and simplifies conceptual understanding while staying mathematically equivalent. However, due to the explicit fourth PSP-Block it gives up the performance boost.

Todo possibly the backend-graph-optimization takes care of this?
maybe check this later on...

3.1.2 Implementation of Subpopulations

The subpopulation concept proposed by David and Friston can be easily implemented in PyRates. Fig. 3.2 shows the necessary adjustments to the operator template.

```

1 rpo_e = OperatorTemplate(
2     name='RP0_e', path=None,
3     equations=[
4         #-----
5         # Subpopulation 0:  $h_0(t)$ 
6         #  $\dot{y}_0 = z_0$ 
7         'd/dt * y_0 = z_0',
8         #  $\dot{z}_0 = \frac{H_0}{\tau_0} x - \frac{2}{\tau_0} z_0 - \frac{1}{\tau_0} y_0^2$ 
9         'd/dt * z_0 = H_0/tau_0 * x - 2./tau_0 * z_0 - (1./tau_0)^2. * y_0',
10        #-----
11        # Subpopulation 1:  $h_1(t)$ 
12        #  $\dot{y}_1 = z_1$ 
13        'd/dt * y_1 = z_1',
14        #  $\dot{z}_1 = \frac{H_1}{\tau_1} x - \frac{2}{\tau_1} z_1 - \frac{1}{\tau_1} y_1^2$ 
15        'd/dt * z_1 = H_1/tau_1 * x - 2./tau_1 * z_1 - (1./tau_1)^2. * y_1',
16        #-----
17        # Population output:
18        #  $y = \sum_{n=0}^N (w_n y_n)$ 
19        'PSP = w_0*y_0 + w_1*y_1'
20        #-----
21    ],
22    variables={
23        'PSP': {'default': 'output'},
24        **{var: {'default': 'variable'} for var in ['y_0', 'y_1', 'z_0', 'z_1']},
25        'x': {'default': 'input'},
26        'w_0': {'default': 1.0},
27        'w_1': {'default': 0.0},
28        'tau_0': {'default': tau_0},
29        'tau_1': {'default': tau_1},
30        'H_0': {'default': h_0},
31        'H_1': {'default': h_1}},
32    description="rate-to-potential operator")

```

Figure 3.2: PSP Block with two subpopulations in PyRates

3.2 Simulating the effects of propofol

3.3 Implementing decay-time modulation

To simulate the effects of propofol on the GABA_A receptors, the IPSP (inhibitory response function h_i) time-constant τ_i is increased by a factor λ [22]:

$$h_i(t) = \frac{H_i}{\lambda \cdot \tau_i} t e^{-\frac{1}{\lambda \cdot \tau_i}}$$

The effect of increasing λ for h_{i_1} and h_{i_2} is visualized in Fig. 3.3.

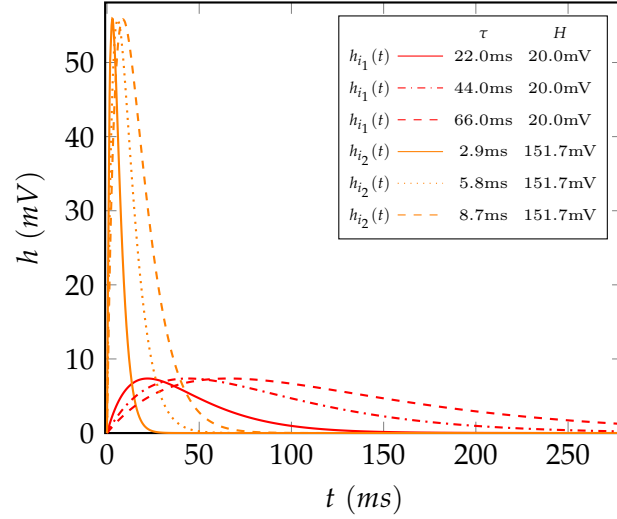


Figure 3.3: Inhibitory PSP functions with varying λ :

The duration of the effect increases while the amplitude stays constant, effectively increasing the charge transfer. (λ in [1.0 (no drug-effect, solid lines), 2.0 (dotted), 3.0 (dashed)])

Varying λ between 1 (0 μM) and 3.0 ($\sim 30 \mu\text{M}$) appears to be a sensible choice for the clinically relevant range, given Fig. 2.1.

Chapter 4

Results

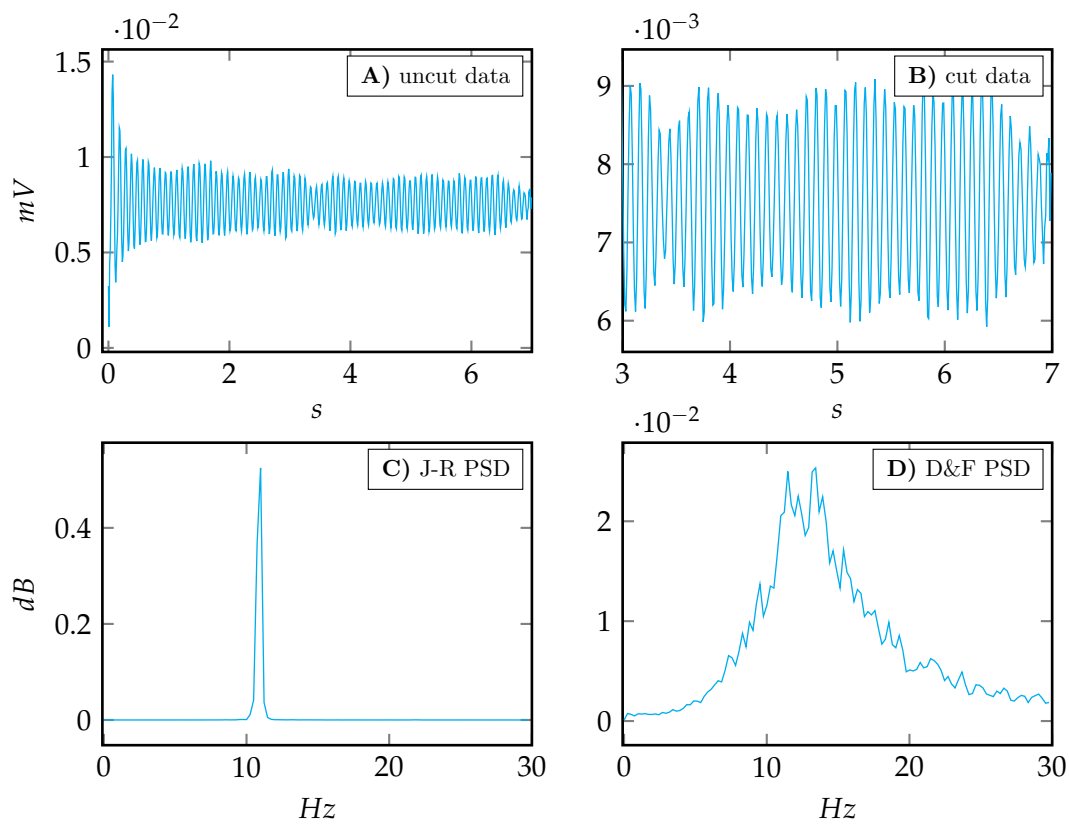


Figure 4.1: Processing of simulated data.

A) & B): removing initially unstable signal by cutting off the first 3s of the data (generated by Simple Jansen-Rit Model with $C = 135$).

C) & D): Power Spectral Density of Jansen-Rit and David & Friston Model (Welch's Method)

4.1 Simulating over the parameter space

When simulating over the selected parameter space $\lambda \in [1, 3]$ (see Fig ?? A), the following phenomena can be observed:

4.1.1 Basic JR Model

1. Increasing λ , from 1.0 first leads to a slight decrease in signal voltage, while roughly maintaining oscillation-amplitude (Fig ?? B). Additionally, the dominant frequencies are in the 10 – 12Hz range Overall the system appears to be in a stable state.
2. Starting from $\lambda \sim 1.1$, the system enters an unstable state, oscillating heavily and dramatically increasing signal amplitude and frequency amplitudes at multiple new peaks around 0 – 10, 12 – 20 and 30 Hz. Further increasing λ shifts the frequency peaks of the disturbed signal slowly towards lower frequencies.
3. At $\lambda \sim 2.05$, the disturbances disappear again, with the system having apparently reached a different stable state. The dominant frequencies have jumped below 2 – 3 Hz,
4. and there is only low-amplitude activity in frequencies above that.
5. Up to $\lambda = 3.0$, the signal voltage slowly continues to slightly decrease as before, however the frequency distribution appears to have settled. Maintaining peak dosage has no further effects.
6. Decreasing from $\lambda = 3.0$ has the expected reverse effect: only the signal voltage slightly increases as well.
7. At $\lambda \sim 1.95$ (somewhat lower than 2.05!), disturbances begin to form again. The system undergoes similar effects in reverse as it did in the other direction.

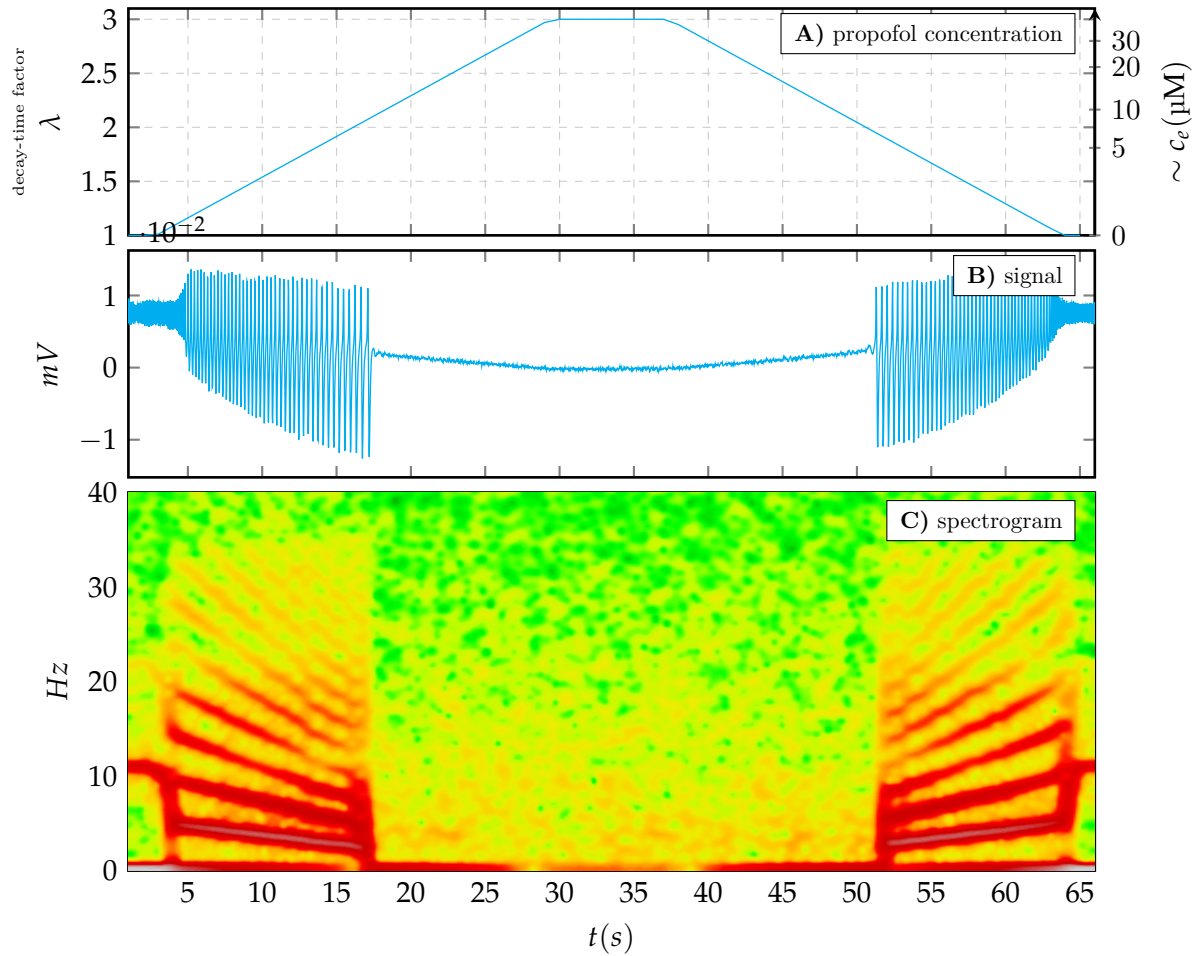


Figure 4.2: Simulation of a sedation:

A): timeline of the simulated IPSP stretch factor λ (roughly representing c_e)

B): timeline of the simulated signal

C): spectrogram

4.1.2 David Friston Extension

1. Steadily increasing λ , from 1.0 first leads to a slight decrease in signal voltage, while roughly maintaining oscillation-amplitude (Fig ?? B). Additionally, the dominant frequencies from the 10 – 12Hz range slowly shift towards
2. 5 – 10Hz (C). Overall the system appears to be in a stable state.
3. Starting from $\lambda \sim 1.85$, the system enters an unstable state, oscillating heavily and dramatically increasing signal amplitude and frequency amplitudes below 25Hz. Further increasing λ has the same minimal effects on the disturbed signal, as the increase had before exiting the stable state.
4. At $\lambda \sim 2.05$, the disturbances disappear again, with the system having apparently reached a different stable state at visibly lower voltage. The dominant frequencies have jumped below 10 Hz.
5. Up to $\lambda = 3.0$, the signal voltage slowly continues to decrease as before, however the frequency distribution appears to have settled. Maintaining peak dosage has no further effects.

6. Decreasing from $\lambda = 3.0$ has the expected reverse effect: only the signal voltage increases as well.
7. At $\lambda \sim 1.95$ (somewhat lower than 2.05!), disturbances begin to form again. The system undergoes similar effects in reverse as it did in the other direction. Noteworthy is however, that the unstable state prevails until λ reaches ~ 1.48 .

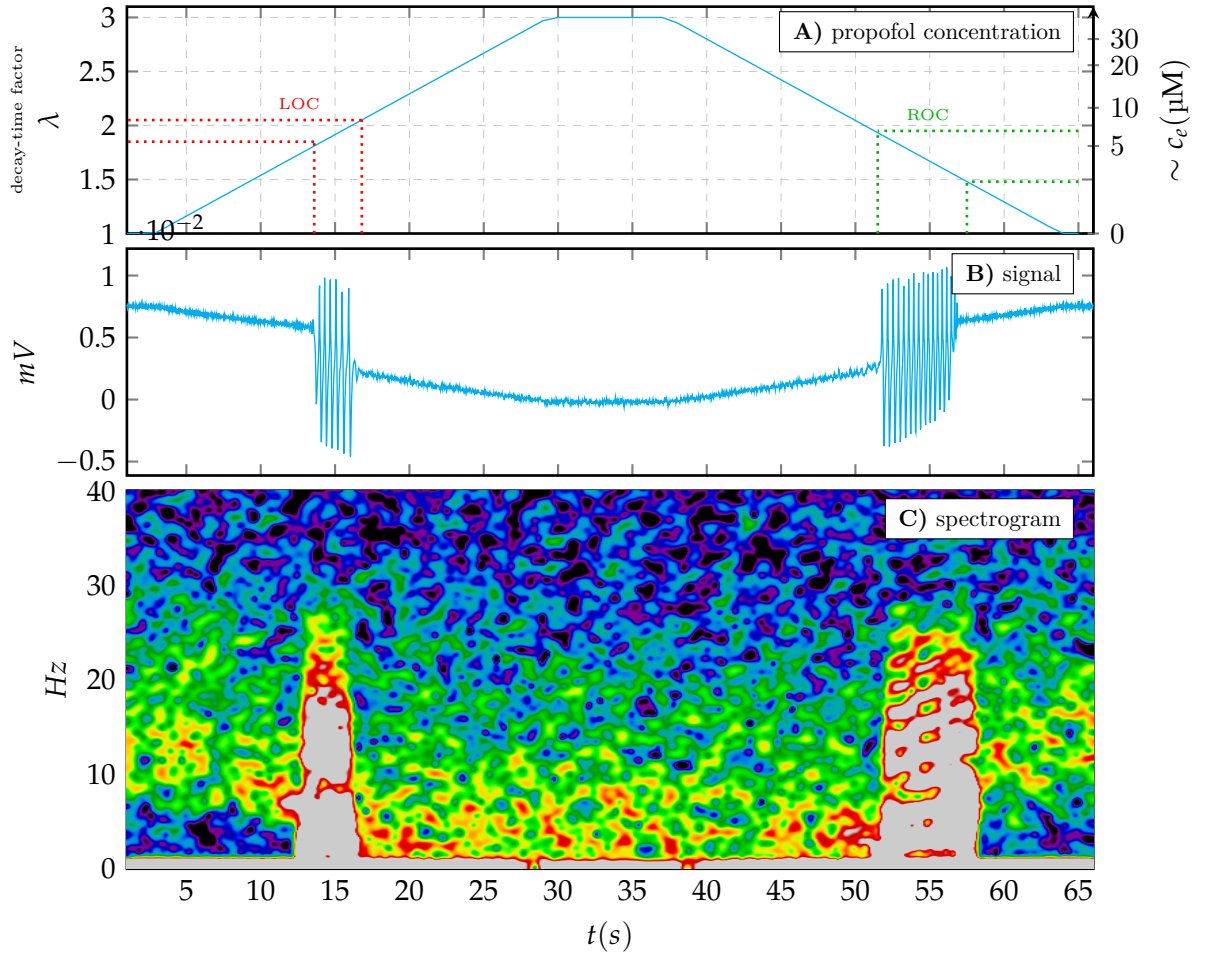


Figure 4.3: Simulation of a sedation:

A): timeline of the simulated IPSP stretch factor λ (roughly representing c_e)

B): timeline of the simulated signal

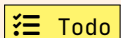
C): spectrogram

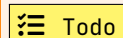
Chapter 5

Discussion

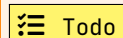
While the NMM used for simulation is a very rough abstraction of cortical dynamics, multiple parallels to effects observed during GA can be drawn:

1. Two, distinguishable **stable states** can be observed. The frequency changes bear strong similarities to the switch to unconsciousness in GA [26], [27].
2. Induction and Emergence are asymmetrical (**hysteresis**). The system predicts that the state-change ‘LOC’ occurs at higher concentrations than ‘ROC’.
3. During state transitions, there is a strong **biphasic effect**. The system predicts that the frequency range below 25Hz receives a temporary amplitude boost during the phase transitions, which disappears while the parameter changes continue in the same direction.
4. In the ‘unconscious’ state, frequency distribution stabilizes independent of further increasing decay-time (**slow-wave-activity saturation?** [26]).

 **Todo** elaborate on all of the above...

 **Todo** draw parallels to [24], which discusses mainly the same effects, although with a different NMM (or ‘mean-field-model’)...

5.1 Outlook

 **Todo** How could the model be extended

Bibliography

- [1] A. Mosso, *Ueber den Kreislauf des Blutes im menschlichen Gehirn ...* de. Veit, 1881.
- [2] H. R. Wilson and J. D. Cowan, “Excitatory and Inhibitory Interactions in Localized Populations of Model Neurons,” en, *Biophysical Journal*, vol. 12, no. 1, pp. 1–24, Jan. 1972, ISSN: 00063495. DOI: [10.1016/S0006-3495\(72\)86068-5](https://doi.org/10.1016/S0006-3495(72)86068-5). [Online]. Available: <https://linkinghub.elsevier.com/retrieve/pii/S0006349572860685> (visited on 10/23/2021).
- [3] F. H. Lopes da Silva, A. Hoeks, H. Smits, and L. H. Zetterberg, “Model of brain rhythmic activity: The alpha-rhythm of the thalamus,” en, *Kybernetik*, vol. 15, no. 1, pp. 27–37, 1974, ISSN: 0340-1200, 1432-0770. DOI: [10.1007/BF00270757](https://doi.org/10.1007/BF00270757). [Online]. Available: <http://link.springer.com/10.1007/BF00270757> (visited on 08/20/2021).
- [4] F. Lopes da Silva, A. van Rotterdam, P. Barts, E. van Heusden, and W. Burr, “Models of Neuronal Populations: The Basic Mechanisms of Rhythmicity,” en, in *Progress in Brain Research*, vol. 45, Elsevier, 1976, pp. 281–308, ISBN: 978-0-444-41457-1. DOI: [10.1016/S0079-6123\(08\)60995-4](https://doi.org/10.1016/S0079-6123(08)60995-4). [Online]. Available: <https://linkinghub.elsevier.com/retrieve/pii/S0079612308609954> (visited on 10/10/2021).
- [5] L. H. Zetterberg, L. Kristiansson, and K. Mossberg, “Performance of a model for a local neuron population,” en, *Biological Cybernetics*, vol. 31, no. 1, pp. 15–26, 1978, ISSN: 0340-1200, 1432-0770. DOI: [10.1007/BF00337367](https://doi.org/10.1007/BF00337367). [Online]. Available: <http://link.springer.com/10.1007/BF00337367> (visited on 10/10/2021).
- [6] G. Bauer, F. Gerstenbrand, and E. Rumpl, “Varieties of the locked-in syndrome,” en, *Journal of Neurology*, vol. 221, no. 2, pp. 77–91, Aug. 1979, ISSN: 0340-5354, 1432-1459. DOI: [10.1007/BF00313105](https://doi.org/10.1007/BF00313105). [Online]. Available: <http://link.springer.com/10.1007/BF00313105> (visited on 06/02/2022).
- [7] A van Rotterdam, F. H. Lopes da Silva, and J van den Ende, “A model of the spatial-temporal characteristics of the alpha rhythm,” en, *Bulletin of Mathematical Biology*, vol. 44, no. 2, pp. 283–305, 1982.
- [8] B. H. Jansen, G. Zouridakis, and M. E. Brandt, “A neurophysiologically-based mathematical model of flash visual evoked potentials,” en, *Biological Cybernetics*, vol. 68, no. 3, pp. 275–283, Jan. 1993, ISSN: 0340-1200, 1432-0770. DOI: [10.1007/BF00224863](https://doi.org/10.1007/BF00224863). [Online]. Available: <http://link.springer.com/10.1007/BF00224863> (visited on 11/27/2020).
- [9] J. C. Sigl and N. G. Chamoun, “An introduction to bispectral analysis for the electroencephalogram,” en, *Journal of Clinical Monitoring*, vol. 10, no. 6, pp. 392–404, Nov. 1994, ISSN: 0748-1977. DOI: [10.1007/BF01618421](https://doi.org/10.1007/BF01618421). [Online]. Available: <http://link.springer.com/10.1007/BF01618421> (visited on 06/12/2022).

- [10] B. H. Jansen and V. G. Rit, "Electroencephalogram and visual evoked potential generation in a mathematical model of coupled cortical columns," en, p. 10, 1995.
- [11] K. Kuizenga, C. J. Kalkman, and P. J. Hennis, "Quantitative electroencephalographic analysis of the biphasic concentration-effect relationship of propofol in surgical patients during extradural analgesia," en, *British Journal of Anaesthesia*, vol. 80, no. 6, pp. 725–732, Jun. 1998, ISSN: 00070912. DOI: [10.1093/bja/80.6.725](https://doi.org/10.1093/bja/80.6.725). [Online]. Available: <https://linkinghub.elsevier.com/retrieve/pii/S0007091217403795> (visited on 05/27/2022).
- [12] D. T. Liley, P. J. Cadusch, and J. J. Wright, "A continuum theory of electrocortical activity," en, *Neurocomputing*, vol. 26-27, pp. 795–800, Jun. 1999, ISSN: 09252312. DOI: [10.1016/S0925-2312\(98\)00149-0](https://doi.org/10.1016/S0925-2312(98)00149-0). [Online]. Available: <https://linkinghub.elsevier.com/retrieve/pii/S0925231298001490> (visited on 06/12/2022).
- [13] F. Wendling, J. J. Bellanger, F. Bartolomei, and P. Chauvel, "Relevance of nonlinear lumped-parameter models in the analysis of depth-EEG epileptic signals," en, *Biological Cybernetics*, vol. 83, no. 4, pp. 367–378, Sep. 2000, ISSN: 0340-1200, 1432-0770. DOI: [10.1007/s004220000160](https://doi.org/10.1007/s004220000160). [Online]. Available: <http://link.springer.com/10.1007/s004220000160> (visited on 06/15/2022).
- [14] K. Kuizenga, "Biphasic EEG changes in relation to loss of consciousness during induction with thiopental, propofol, etomidate, midazolam or sevoflurane," en, p. 7, 2001.
- [15] M. Steriade, "Impact of Network Activities on Neuronal Properties in Corticothalamic Systems," en, *Journal of Neurophysiology*, vol. 86, no. 1, pp. 1–39, Jul. 2001, ISSN: 0022-3077, 1522-1598. DOI: [10.1152/jn.2001.86.1.1](https://doi.org/10.1152/jn.2001.86.1.1). [Online]. Available: <https://www.physiology.org/doi/10.1152/jn.2001.86.1.1> (visited on 01/09/2022).
- [16] O. David and K. J. Friston, "A neural mass model for MEG/EEG: Coupling and neuronal dynamics," en, *NeuroImage*, vol. 20, no. 3, pp. 1743–1755, Nov. 2003, ISSN: 1053-8119. DOI: [10.1016/j.neuroimage.2003.07.015](https://doi.org/10.1016/j.neuroimage.2003.07.015). [Online]. Available: <http://www.sciencedirect.com/science/article/pii/S1053811903004579> (visited on 12/04/2020).
- [17] A. Kitamura, W. Marszalec, J. Z. Yeh, and T. Narahashi, "Effects of Halothane and Propofol on Excitatory and Inhibitory Synaptic Transmission in Rat Cortical Neurons," en, *Journal of Pharmacology and Experimental Therapeutics*, vol. 304, no. 1, pp. 162–171, Jan. 2003, ISSN: 0022-3565, 1521-0103. DOI: [10.1124/jpet.102.043273](https://doi.org/10.1124/jpet.102.043273). [Online]. Available: <http://jpet.aspetjournals.org/lookup/doi/10.1124/jpet.102.043273> (visited on 05/26/2022).
- [18] M. L. Steyn-Ross, D. Steyn-Ross, and J. Sleight, "Modelling general anaesthesia as a first-order phase transition in the cortex," en, *Progress in Biophysics and Molecular Biology*, vol. 85, no. 2-3, pp. 369–385, Jun. 2004, ISSN: 00796107. DOI: [10.1016/j.pbiomolbio.2004.02.001](https://doi.org/10.1016/j.pbiomolbio.2004.02.001). [Online]. Available: <https://linkinghub.elsevier.com/retrieve/pii/S0079610704000264> (visited on 10/23/2021).
- [19] H. Iwakiri, N. Nishihara, O. Nagata, T. Matsukawa, M. Ozaki, and D. I. Sessler, "Individual Effect-Site Concentrations of Propofol Are Similar at Loss of Consciousness and at Awakening," en, *Anesthesia & Analgesia*, vol. 100, no. 1, pp. 107–110, Jan. 2005, ISSN: 0003-2999. DOI: [10.1213/01.ANE.0000139358](https://doi.org/10.1213/01.ANE.0000139358).

- 15909.EA. [Online]. Available: <http://journals.lww.com/00000539-200501000-00021> (visited on 05/20/2022).
- [20] S. J. McDougall, T. W. Bailey, D. Mendelowitz, and M. C. Andresen, "Propofol enhances both tonic and phasic inhibitory currents in second-order neurons of the solitary tract nucleus (NTS)," en, *Neuropharmacology*, vol. 54, no. 3, pp. 552–563, Mar. 2008, ISSN: 00283908. DOI: [10.1016/j.neuropharm.2007.11.001](https://doi.org/10.1016/j.neuropharm.2007.11.001). [Online]. Available: <https://linkinghub.elsevier.com/retrieve/pii/S0028390807003516> (visited on 05/27/2022).
- [21] R. Moran, K. Stephan, T. Seidenbecher, H.-C. Pape, R. Dolan, and K. Friston, "Dynamic causal models of steady-state responses," en, *NeuroImage*, vol. 44, no. 3, pp. 796–811, Feb. 2009, ISSN: 10538119. DOI: [10.1016/j.neuroimage.2008.09.048](https://doi.org/10.1016/j.neuroimage.2008.09.048). [Online]. Available: <https://linkinghub.elsevier.com/retrieve/pii/S1053811908010641> (visited on 06/15/2022).
- [22] A. Hutt and A. Longtin, "Effects of the anesthetic agent propofol on neural populations," en, *Cognitive Neurodynamics*, vol. 4, no. 1, pp. 37–59, Mar. 2010, ISSN: 1871-4080, 1871-4099. DOI: [10.1007/s11571-009-9092-2](https://doi.org/10.1007/s11571-009-9092-2). [Online]. Available: <http://link.springer.com/10.1007/s11571-009-9092-2> (visited on 03/22/2022).
- [23] A. Spiegler, S. J. Kiebel, F. M. Atay, and T. R. Knösche, "Bifurcation analysis of neural mass models: Impact of extrinsic inputs and dendritic time constants," en, *NeuroImage*, vol. 52, no. 3, pp. 1041–1058, Sep. 2010, ISSN: 10538119. DOI: [10.1016/j.neuroimage.2009.12.081](https://doi.org/10.1016/j.neuroimage.2009.12.081). [Online]. Available: <https://linkinghub.elsevier.com/retrieve/pii/S1053811909013706> (visited on 06/16/2022).
- [24] D. A. Steyn-Ross, M. L. Steyn-Ross, J. W. Sleight, and M. T. Wilson, "Progress in Modeling EEG Effects of General Anesthesia: Biphasic Response and Hysteresis," en, in *Sleep and Anesthesia*, A. Hutt, Ed., New York, NY: Springer New York, 2011, pp. 167–194, ISBN: 978-1-4614-0172-8 978-1-4614-0173-5. DOI: [10.1007/978-1-4614-0173-5_8](https://doi.org/10.1007/978-1-4614-0173-5_8). [Online]. Available: http://link.springer.com/10.1007/978-1-4614-0173-5_8 (visited on 05/26/2022).
- [25] A. G. Casali, O. Gosseries, M. Rosanova, *et al.*, "A Theoretically Based Index of Consciousness Independent of Sensory Processing and Behavior," en, *Science Translational Medicine*, vol. 5, no. 198, Aug. 2013, ISSN: 1946-6234, 1946-6242. DOI: [10.1126/scitranslmed.3006294](https://doi.org/10.1126/scitranslmed.3006294). [Online]. Available: <https://www.science.org/doi/10.1126/scitranslmed.3006294> (visited on 06/12/2022).
- [26] R. Ní Mhuirheartaigh, C. Warnaby, R. Rogers, S. Jbabdi, and I. Tracey, "Slow-Wave Activity Saturation and Thalamocortical Isolation During Propofol Anesthesia in Humans," en, *Science Translational Medicine*, vol. 5, no. 208, Oct. 2013, ISSN: 1946-6234, 1946-6242. DOI: [10.1126/scitranslmed.3006007](https://doi.org/10.1126/scitranslmed.3006007). [Online]. Available: <https://www.science.org/doi/10.1126/scitranslmed.3006007> (visited on 05/28/2022).
- [27] P. L. Purdon, E. T. Pierce, E. A. Mukamel, *et al.*, "Electroencephalogram signatures of loss and recovery of consciousness from propofol," en, *MEDICAL SCIENCES*, p. 10, 2013.
- [28] I. Bojak, "Neural Population Models and Cortical Field Theory: Overview," en, in *Encyclopedia of Computational Neuroscience*, D. Jaeger and R. Jung, Eds., New York, NY: Springer New York, 2014, pp. 1–3, ISBN: 978-1-4614-7320-6. DOI: [10.1007/978-1-4614-7320-6_759-1](https://doi.org/10.1007/978-1-4614-7320-6_759-1). [Online]. Available: [http :](http://)

- [//link.springer.com/10.1007/978-1-4614-7320-6_759-1](http://link.springer.com/10.1007/978-1-4614-7320-6_759-1) (visited on 06/15/2022).
- [29] F. Cona, M. Lacanna, and M. Ursino, “A thalamo-cortical neural mass model for the simulation of brain rhythms during sleep,” en, *Journal of Computational Neuroscience*, vol. 37, no. 1, pp. 125–148, Aug. 2014, ISSN: 0929-5313, 1573-6873. DOI: [10.1007/s10827-013-0493-1](https://doi.org/10.1007/s10827-013-0493-1). [Online]. Available: <http://link.springer.com/10.1007/s10827-013-0493-1> (visited on 06/12/2022).
 - [30] D. J. Eleveld, J. H. Proost, L. I. Cortínez, A. R. Absalom, and M. M. R. F. Struys, “A General Purpose Pharmacokinetic Model for Propofol,” en, *Anesthesia & Analgesia*, vol. 118, no. 6, pp. 1221–1237, Jun. 2014, ISSN: 0003-2999. DOI: [10.1213/ANE.000000000000165](https://doi.org/10.1213/ANE.000000000000165). [Online]. Available: <https://journals.lww.com/00000539-201406000-00012> (visited on 05/28/2022).
 - [31] T. R. Knösche, “Jansen-Rit Model,” en, in *Encyclopedia of Computational Neuroscience*, D. Jaeger and R. Jung, Eds., New York, NY: Springer New York, 2014, pp. 1–5, ISBN: 978-1-4614-7320-6. DOI: [10.1007/978-1-4614-7320-6_65-2](https://doi.org/10.1007/978-1-4614-7320-6_65-2). [Online]. Available: http://link.springer.com/10.1007/978-1-4614-7320-6_65-2 (visited on 06/15/2022).
 - [32] Z. Liang, X. Duan, C. Su, L. Voss, J. Sleight, and X. Li, “A Pharmacokinetics-Neural Mass Model (PK-NMM) for the Simulation of EEG Activity during Propofol Anesthesia,” en, *PLOS ONE*, vol. 10, no. 12, D. Marinazzo, Ed., e0145959, Dec. 2015, ISSN: 1932-6203. DOI: [10.1371/journal.pone.0145959](https://doi.org/10.1371/journal.pone.0145959). [Online]. Available: <https://dx.plos.org/10.1371/journal.pone.0145959> (visited on 10/23/2021).
 - [33] E. Montbrió, D. Pazó, and A. Roxin, “Macroscopic Description for Networks of Spiking Neurons,” en, *Physical Review X*, vol. 5, no. 2, p. 021028, Jun. 2015, ISSN: 2160-3308. DOI: [10.1103/PhysRevX.5.021028](https://doi.org/10.1103/PhysRevX.5.021028). [Online]. Available: <https://link.aps.org/doi/10.1103/PhysRevX.5.021028> (visited on 01/09/2022).
 - [34] L. Kuhlmann, D. R. Freestone, J. H. Manton, *et al.*, “Neural mass model-based tracking of anesthetic brain states,” en, *NeuroImage*, vol. 133, pp. 438–456, Jun. 2016, ISSN: 10538119. DOI: [10.1016/j.neuroimage.2016.03.039](https://doi.org/10.1016/j.neuroimage.2016.03.039). [Online]. Available: <https://linkinghub.elsevier.com/retrieve/pii/S1053811916002445> (visited on 06/12/2022).
 - [35] P. O. Sepúlveda, E. Carrasco, L. F. Tapia, *et al.*, “Evidence of hysteresis in propofol pharmacodynamics,” en, *Anaesthesia*, vol. 73, no. 1, pp. 40–48, Jan. 2018, ISSN: 00032409. DOI: [10.1111/anae.14009](https://doi.org/10.1111/anae.14009). [Online]. Available: <https://onlinelibrary.wiley.com/doi/10.1111/anae.14009> (visited on 05/26/2022).
 - [36] S. Bensaid, J. Modolo, I. Merlet, F. Wendling, and P. Benquet, “COALIA: A Computational Model of Human EEG for Consciousness Research,” English, *Frontiers in Systems Neuroscience*, vol. 13, 2019, Publisher: Frontiers, ISSN: 1662-5137. DOI: [10.3389/fnsys.2019.00059](https://doi.org/10.3389/fnsys.2019.00059). [Online]. Available: <https://www.frontiersin.org/articles/10.3389/fnsys.2019.00059/full> (visited on 06/14/2020).
 - [37] R. Gast, D. Rose, C. Salomon, H. E. Möller, N. Weiskopf, and T. R. Knösche, “PyRates—A Python framework for rate-based neural simulations,” en, *PLOS ONE*, vol. 14, no. 12, e0225900, Dec. 2019, Publisher: Public Library of Science, ISSN: 1932-6203. DOI: [10.1371/journal.pone.0225900](https://doi.org/10.1371/journal.pone.0225900). [Online]. Available: <https://journals.plos.org/plosone/article?id=10.1371/journal.pone.0225900> (visited on 11/27/2020).

- [38] A. L. Ferreira, R. Correia, S. Vide, *et al.*, “Patterns of Hysteresis Between Induction and Emergence of Neuroanesthesia Are Present in Spinal and Intracranial Surgeries,” en, *Journal of Neurosurgical Anesthesiology*, vol. 32, no. 1, pp. 82–89, Jan. 2020, ISSN: 0898-4921. DOI: [10.1097/ANA.0000000000000559](https://doi.org/10.1097/ANA.0000000000000559). [Online]. Available: <https://journals.lww.com/10.1097/ANA.0000000000000559> (visited on 05/27/2022).
- [39] C.-W. Su, L. Zheng, Y.-J. Li, *et al.*, “Hysteresis in anesthesia and recovery: Experimental observation and dynamical mechanism,” en, *Physical Review Research*, vol. 2, no. 2, p. 023 289, Jun. 2020, ISSN: 2643-1564. DOI: [10.1103/PhysRevResearch.2.023289](https://doi.org/10.1103/PhysRevResearch.2.023289). [Online]. Available: <https://link.aps.org/doi/10.1103/PhysRevResearch.2.023289> (visited on 05/28/2022).
- [40] N. Deschle, J. Ignacio Gossn, P. Tewarie, B. Schelter, and A. Daffertshofer, “On the Validity of Neural Mass Models,” *Frontiers in Computational Neuroscience*, vol. 14, p. 118, 2021, ISSN: 1662-5188. DOI: [10.3389/fncom.2020.581040](https://doi.org/10.3389/fncom.2020.581040). [Online]. Available: <https://www.frontiersin.org/article/10.3389/fncom.2020.581040> (visited on 08/20/2021).
- [41] M. R. Panahi, G. Abrevaya, J.-C. Gagnon-Audet, V. Voleti, I. Rish, and G. Dumas, *Generative Models of Brain Dynamics – A review*, en, Number: arXiv:2112.12147 arXiv:2112.12147 [q-bio], Dec. 2021. [Online]. Available: <http://arxiv.org/abs/2112.12147> (visited on 06/12/2022).
- [42] S. Jain and L. M. Iverson, “Glasgow Coma Scale,” eng, in *StatPearls*, Treasure Island (FL): StatPearls Publishing, 2022. [Online]. Available: <http://www.ncbi.nlm.nih.gov/books/NBK513298/> (visited on 06/12/2022).
- [43] S. Mathur, J. Patel, S. Goldstein, and A. Jain, “Bispectral Index,” eng, in *StatPearls*, Treasure Island (FL): StatPearls Publishing, 2022. [Online]. Available: <http://www.ncbi.nlm.nih.gov/books/NBK539809/> (visited on 06/12/2022).